THE JOURNAL OF PHYSICAL CHEMISTRY B

Article

pubs.acs.org/JPCB

# Evaluation of the Cross Section of Elongated Micelles by Static and Dynamic Light Scattering

Gerald Guerin,[†] Fei Qi,[†] Graeme Cambridge,[†] Ian Manners,*[,‡] and Mitchell A. Winnik*[,†]

[†]Department of Chemistry, University of Toronto, 80 St. George Street, Toronto, ON, M5S 1H6

[‡]School of Chemistry, University of Bristol, Bristol U.K., BS8 1TS

Supporting Information

**ABSTRACT:** We describe simultaneous static (SLS) and dynamic light scattering (DLS) measurements on dilute solutions of a series of poly(ferrocenyldimethylsilane-*b*-isoprene) ($PFS_{50}$–$PI_{1000}$) block copolymer micelles of uniform length in *tert*-butyl acetate (*t*BA) and in decane. The subscripts in the term $PFS_{50}$–$PI_{1000}$ refer to the mean degree of polymerization of each block. The SLS experiments show that in both solvents the micelles formed are elongated and rigid. We also observed that the large length of the PI block (1000 units) contributes to the SLS signal. From the SLS data, we calculated the mass per unit length (linear aggregation number), as well as the cross section of the micelles in both solvents. Interestingly, the linear aggregation number and the micelle cross sections, as deduced by SLS, were the same in decane and in *t*BA. However, the fitting of DLS data indicates that the hydrodynamic cross section of the micelles in *t*BA is much larger than that in decane, and both values are larger than the values determined by SLS. We hypothesize that the difference between cross sections deduced from SLS and DLS data fitting is related to the shape of the segment density profile of the corona. In *t*BA, the PI chains are more stretched than in decane, increasing the hydrodynamic radius of the micelle cross section.

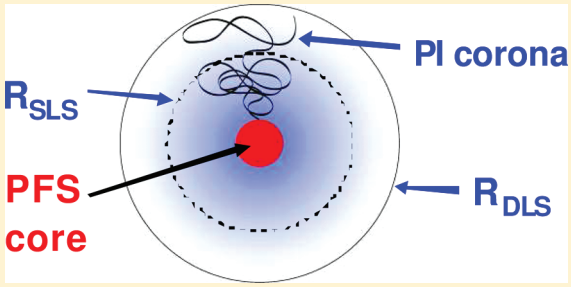


## INTRODUCTION

Block copolymers self-assemble in selective solvents to form micelles with an insoluble core, surrounded by a solvent swollen corona.[1,2] The shape of the micelles is dictated primarily by the ratio of the number of segments in each block but is also affected by the choice of solvent if the solvent can swell the core. If the core-forming block is an amorphous polymer ("coil–coil" block copolymers), the most common morphology obtained is spherical.[3−5] Cylinders[6] are obtained for a very narrow range of compositions for blocks of similar length, and vesicles[7] are obtained only for a somewhat broader range of block ratios. However, when the insoluble block forms a semicrystalline core ("crystalline–coil" block copolymers), thin lamellae and elongated structures are the predominant morphologies observed.[8,9] Cylindrical micelles are currently of great interest because of their widespread applications in different fields. Examples include flow-intensive drug delivery,[10] as additives for the enhancement of the toughness of epoxy resin[11] and as scaffolds or templates for the deposition of metal nanoparticles.[12] In parallel, there has been a growing interest in crystalline–coil block copolymers that form elongated micelles.[13−21] We have used the term "crystallization-driven self assembly" to describe block copolymer self-assembly where the structures formed are a consequence of the crystallization of the insoluble block.[16]

We have been particularly interested in the formation of elongated micelles by polyferrocenyldimethylsilane (PFS) block copolymers.[13−17] The polymers undergo crystallization-driven self-assembly in solvents selective for the non-PFS block. Examples include PFS–PDMS (PDMS = polydimethylsiloxane) and PFS–PI (PI = polyisoprene) in decane or *n*-hexane. One of the features that distinguish the formation of elongated micelles by PFS block copolymers is that these micelles undergo seeded growth. If one adds a concentrated solution of unimer to a solution of PFS block copolymer micelles in a selective solvent, the new polymer does not form new micelles. Rather, it deposits onto the ends of existing micelles, a process that resembles epitaxial growth. If the seed micelles are obtained (for example, by sonication) with a narrow length distribution, then the micelles obtained also have a narrow length distribution, with values of the weight-average-to-number-average length ($L_w/L_n$) on the order of 1.01.

The contour lengths of one-dimensional micelles are normally characterized using imaging techniques[22] such as transmission electron microscopy (TEM),[23] fluorescence microscopy,[24] or atomic force microscopy (AFM).[25] However, more information can be obtained with scattering techniques. For example, static light scattering (SLS) can be used to determine the length of elongated structures,[26,27] whether they are rigid or flexible,[28] and their mass per unit length. Small angle X-ray (SAXS),[229,30] and neutron (SANS)[31] scattering can also provide information about the mass per unit length, as well

Received: October 31, 2011
Revised: February 28, 2012
Published: March 26, 2012

as information about the size of the micelle cross section. Finally, dynamic light scattering (DLS) has been widely used to evaluate the hydrodynamic cross section of natural fibrils[32−36] and elongated micelles.[37]

We are interested in characterizing elongated micelles with a crystalline core using static and dynamic light scattering. In a previous publication, we reported SLS and DLS studies of cylindrical micelles formed by $PFS_{40}$−$PDMS_{480}$ (the subscripts refer to the number average degree of polymerization) in decane.[37] These micelles had a PFS core and a PDMS corona. Since PDMS and decane have similar values of the refractive index (1.41), the micelle corona was contrast matched and did not scatter light. In this case, the variation of the scattered intensity as a function of scattering angle could be well fitted by the form factor of a long thin rigid rod, confirming that the corona had no effect on the scattered signal. However, because the corona affects the diffusion of the micelles, we could evaluate the hydrodynamic radius of the micelle cross section by DLS. More recently, we studied cylindrical micelles formed by $PFS_{48}$−$PI_{264}$ in decane by SLS.[38] Here, too, we could fit the scattering data to the form factor of a thin rigid rod. Although one anticipates scattering contrast from PI in decane, the contribution of the corona to the scattering signal could not be detected, probably because the corona was too short.

In this paper, we report a light scattering study of elongated micelles obtained by seeded growth of $PFS_{50}$−$PI_{1000}$ micelles in *tert*-butyl acetate (*t*BA) and in decane.[39] Seeded growth experiments allowed us to control precisely the final length of the micelles.[40] The long PI block (1000 units) should make a substantial contribution to the cross section of these micelles. We performed SLS measurements on a series of micelles of different length to examine how the corona chains affect the scattered signal of the elongated micelles at different scattering angles. From the fitting of these results, we could evaluate the radius of the micelle cross section, $R_{SLS}$. These data were then compared to the hydrodynamic radius of the micelle cross section, $R_{DLS}$, deduced from multiangle DLS measurements. To our knowledge, this is the first time that the cross sections of thick rigid rod samples have been evaluated by both SLS and DLS.

## EXPERIMENTAL SECTION

**Materials.** *tert*-Butyl acetate (*t*BA) (99+%) and decane (99+%) were purchased from Aldrich and used without further purification. The $PFS_{50}$−$PI_{1000}$ block copolymer is the same sample described in ref 39. Disposable 17 mm × 60 mm glass cells for light scattering were purchased from Fisher Scientific Chemicals. Dust was removed from the cells by washing them in an acetone still for 15 min.

**Sample Preparation.** Micelle samples with different lengths were prepared as described elsewhere.[39] Namely, two sets of samples (0.2 mg/mL) were prepared, one in decane and the other in *t*BA, by heating the solutions in an oil bath at 90 °C for 30 min and letting them cool to room temperature in air. After the micelle growth was completed, the solutions were sonicated to prepare seed solutions. The length of the seeds (decane: $L_n$ = 50.9, $L_w$ = 57.0 nm; *t*BA: $L_n$ = 50.8 nm, $L_w$ = 59.2 nm) was evaluated by TEM image analysis.

Sonication experiments were carried out by immersing a sealed vial containing each sample into the water-containing chamber of a 70 W ultrasonic cleaning bath at room temperature. The *t*BA solution was sonicated for a total of 40 min, in four 10 min intervals, while the decane solution was sonicated for only two 10 min intervals. After sonication, the seed solutions in *t*BA and in decane were diluted to 0.02 mg/mL for the growth experiments. The growth experiments were carried out by adding increasing amounts (4, 21, 38, 50, 80, 100 μL) of $PFS_{50}$−$PI_{1000}$ dissolved in tetrahydrofuran (THF, $c$ = 9.3 mg/mL) to 2.0 mL aliquots of sonicated $PFS_{50}$−$PI_{1000}$ micelles in *t*BA or in decane. After swirling to mix each of the growth solutions, they were allowed to age in the dark at room temperature. The length of the micelles was evaluated several weeks later by SLS and compared to the values obtained by TEM.

**Transmission Electron Microscopy.** Bright field TEM micrographs were obtained on a Hitachi H-7000 microscope operating at 100 kV. TEM samples were prepared at room temperature by placing a drop of each solution onto a carbon coated copper grid. Excess fluid was then removed with a clean piece of filter paper. Before every EM session, the electron beam was aligned to minimize optical artifacts. Images were analyzed using the software package Image J, published by the National Institutes of Health. For the statistical length analysis, between 200 and 400 micelles were traced by hand to determine the contour length. The number average micelle length ($L_n$) and weight-average micelle length ($L_w$) were calculated using eq 1, where $N$ is the number of micelles examined in each sample, and $L_i$ is the contour length of the $i$th micelle.

$$L_n = \frac{\sum_{i=1}^{N} N_i L_i}{\sum_{i=1}^{N} N_i} \qquad L_w = \frac{\sum_{i=1}^{N} N_i L_i^2}{\sum_{i=1}^{N} N_i L_i} \tag{1}$$

**Light Scattering Equipments.** Static (SLS) and dynamic light scattering (DLS) measurements were performed using a wide angle light scattering photometer from ALV. The light source was a JDS Uniphase He−Ne laser ($\lambda$ = 632.8 nm, 35 mW) emitting vertically polarized light. The cells were placed into the ALV/DLS/SLS-5000 Compact Goniometer System and sat in a vat of toluene, which matched the index of refraction of the glass cells. The scattered light was detected by a Dual ALV-High Q.E. APD avalanche photodiode module, interfaced to the ALV-5000/EPP multiple tau digital. All measurements were carried out at 20 °C. SLS and DLS experiments were performed simultaneously in an unpolarized configuration, i.e., without any polarizer installed in front of the detector. The angular range consisted of scattering angles between 20 and 150° (at 5° intervals). Toluene was used as the standard in the SLS measurements.

**Sample Preparation for Light Scattering Experiments.** The seeded growth solutions prepared in decane and in *t*BA were diluted to a concentration of ca. 0.02 mg/mL. At this low concentration, all the micelle samples were in the dilute regime, as shown in Figure S1 in the Supporting Information where we plotted the overlap concentration as a function of micelle length and compared this overlap concentration to the concentration of the micelle solutions. The solutions were then injected into a light scattering cell without filtration. Prior to performing light scattering experiments, all of the samples were reweighed and the concentrations recalculated. Due to solvent evaporation and dilution, the amount of THF which might remain in the solution was considered as negligible. All the light scattering experiments were carried out at least 1 week after the addition of the unimer solution in THF to ensure that the growth of the micelles was complete.


dx.doi.org/10.1021/jp210454z | J. Phys. Chem. B 2012, 116, 4328−4337

## THEORY AND DATA ANALYSIS

**Static Light Scattering.** In static light scattering (SLS), one obtains structural and dimensional information by measuring the angular dependence of the excess absolute time-average scattered intensity (the Rayleigh ratio, $R_\theta$). For dilute solutions, $R_\theta$ is related to the sample concentration $c$, the second viral coefficient $A_2$, and the form factor $P(q)$ through the expression

$$\left(\frac{Kc}{R_\theta}\right) = \left[\frac{1}{M_w P(q)} + 2A_2 c + \ldots\right] \tag{2}$$

with $K = 4\pi^2 n_s^2 (dn/dc)^2/(N_A \lambda^4)$, and $N_A$ is Avogadro's number, $\lambda$ is the incident wavelength (632.8 nm), $dn/dc$ is the refractive index increment, and $n_s$ is the refractive index of solvent, i.e., decane ($n_s$ = 1.41) or *t*BA ($n_s$ = 1.386). The $(dn/dc)_{block}$ value of each block of $PI_{1000}$-*b*-$PFS_{50}$ in decane was calculated using the Dale−Gladstone relation: $dn/dc \approx (n_p - n_s)/\rho_p$, where $n_p$ is the refractive index of the polymer constituting block and $\rho_p$ is the density of the polymer. The error in the approximation of $(dn/dc)_{block}$ has been estimated to be lower than 5%.[41] To calculate $(dn/dc)_{block}$, we used a density of 1.26 g/cm$^3$ and a refractive index of 1.68 for the PFS block and a density of 0.92 g/cm$^3$ and a refractive index of 1.52 for the PI block. From these data, we evaluated the refractive increments in decane to be for the PFS block $(dn/dc)_{PFS}^{dec} \approx 0.214$ mL/g and for the PI block $(dn/dc)_{PI}^{dec} \approx 0.120$ mL/g, while, in *t*BA, $(dn/dc)_{PFS}^{tBA} \approx 0.233$ mL/g and $(dn/dc)_{PI}^{tBA} \approx 0.146$ mL/g. The overall copolymer $(dn/dc)_{tot}$ was then deduced from the weighted sum of the polymer blocks $dn/dc$:

$$\left(\frac{dn}{dc}\right)_{tot} = w_{PFS}\left(\frac{dn}{dc}\right)_{PFS} + w_{PI}\left(\frac{dn}{dc}\right)_{PI} \tag{3}$$

where $w_{PFS}$ is the weight fraction of the PFS block ($w_{PFS}$ = 0.151) and $w_{PI}$ is that of the PI block ($w_{PI}$ = 0.849). From the calculated values of the refractive increment of each block of the copolymer in decane or in *t*BA and their weight fraction in the copolymer, we evaluate $(dn/dc)_{tot}^{dec}$ to be 0.134 mL/g in decane and $(dn/dc)_{tot}^{tBA}$ to be 0.159 mL/g in *t*BA.

In the Guinier regime, ($qR_g < 1$, $q = 4\pi n \sin(\theta/2)/\lambda$, and $R_g$ is the square root of the *z*-averaged radius of gyration of the scatterers), the form factor of the scattering objects, $P(q)$, is a linear function of $q^2$: $P(q) = 1 - (q^2 R_g^2)/3$. In this case, $P(q)$ does not depend on the shape of the scattering object, and $R_g$ can be deduced from the tangent of the plot at $q = 0$. The value of the weight average molecular weight of the structure in solution, $M_w$, can be calculated from the intercept at $q = 0$ for data extrapolated to $c = 0$. When the size of the scattering structure is very large, however, it is difficult to have enough data in the Guinier regime to determine $R_g$ and $M_w$, and one has to choose a more appropriate representation to deduce the main characteristics of the scattering structure.

For long thin rigid cylindrical micelles, the mass per unit length of the micelle can be calculated without making any preliminary assumptions,[42] using a Holtzer−Casassa (HC) representation.[26,27] For long thin micelles formed from block copolymers with a narrow molecular weight distribution, we use a slightly modified version of the HC representation, and plot the ratio $qR_\theta/\pi M_0 Kc$ as a function of $q$. As in the traditional HC plot, the slope reaches a plateau value at high $q$, but in our approach to data analysis, the magnitude of the plateau value is equal to the number of polymer molecules per unit length. We refer to this value as the linear aggregation number, $N_{agg/L}$.

**Dynamic Light Scattering.** In a dynamic light scattering experiment, the measured intensity−intensity time-correlation function $g^{(2)}(t_c)$, where $t_c$ is the delay time, is related to the normalized electric field correlation function $g^{(1)}(t_c)$, representative of the motion of the particles, by the Siegert relation:

$$g^{(2)}(t_c) = 1 + \beta |g^{(1)}(t_c)|^2 \tag{4}$$

where $\beta$ (<1) is a spatial coherence coefficient for instrument beating efficiency.[43] As $t_c$ increases, $g^{(1)}(t_c)$ decays. This decay carries information about the diffusion of the particles in solution. For monodisperse spherical particles undergoing Brownian motion, the decay curve can be described by a single exponential term.

$$g^{(1)}(t_c) = \exp(-\Gamma t_c) \tag{5}$$

where the decay rate $\Gamma$ is related to the mutual diffusion coefficient $D_m$ of the diffusing species as $\Gamma = q^2 D_m$. Thus, a plot of $\Gamma$ vs $q^2$ should be linear with slope $D_m$ and pass through the origin. For hard spheres, the apparent hydrodynamic radius, $R_h$, can be evaluated from $D_m$ using the Stokes−Einstein equation:

$$R_h = \frac{k_B T}{6\pi\eta_0 D_m} \tag{6}$$

where $k_B$ is the Boltzmann constant, $T$ is the temperature, and $\eta_0$ is the solvent viscosity.

For polydisperse or rigid extended systems, $g^{(1)}(t_c)$ cannot be described by a single decay rate, $\Gamma$, but by a continuous distribution of decay rates, $G(\Gamma)$. In such a case, $g^{(1)}(t_c)$ is defined as the Laplace transform of the decay rate distribution function $G(\Gamma)$:

$$g^{(1)}(t_c) = \int_0^\infty G(\Gamma) \exp(-\Gamma t_c)\, d\Gamma \tag{7}$$

There are different approaches to extract the average value, $\Gamma_1$, of $g^{(1)}(t_c)$.[44−46] We analyzed our data in terms of a cumulant expansion to second order (2-CUM) of the logarithm of $g^{(1)}(t_c)$, using the ALV correlator software:

$$\ln g^{(1)}(t_c) = -\Gamma_1 t_c + \left(\frac{\mu_2}{2!}\right) t_c^2 \tag{8}$$

where $\Gamma_1$ is also known as the first cumulant, while $\mu_2$ is the second cumulant, which allows one to evaluate the polydispersity of the distribution of decay rates.

For rigid rods, the translational diffusion coefficient parallel to the rod axis, $D_\parallel$, that perpendicular to the rod axis, $D_\perp$, and the rotational diffusion coefficient, $D_r$, all greatly influence the evolution of the first cumulant as a function of the scattering angle. For a dilute solution of rigid rods, when the translational and rotational motions are coupled, Maeda and Fujime have shown that the reduced cumulant, $\Gamma_1/q^2$, can be expressed by eq 9:[47]

$$\Gamma_1/q^2 = \left[D + (L^2/12)\cdot D_r f_1\left(\frac{qL}{2}\right) - (D_\parallel - D_\perp)\cdot \left(1/3 - f_2\left(\frac{qL}{2}\right)\right)\right] \tag{9}$$

where $D$ is the overall translational diffusion coefficient of the rod, defined as $D = (2D_\perp + D_\parallel)/3$. $f_1(qL/2)$ and $(1/3 - f_2(qL/$


dx.doi.org/10.1021/jp210454z | J. Phys. Chem. B 2012, 116, 4328−4337

2)) are weighting factors which depend on $qL/2$ and are given by Maeda and Fujime.[47] When $q$ tends to 0, $f_1(qL/2) = 0$ and $f_2(qL/2) = 1/3$; then, according to eq 9, $\Gamma_1/q^2$ tends to the overall translational diffusion coefficient, $D$.

The translational and rotational diffusion coefficients can be expressed as a function of the ratio of the rod length to the cross-sectional diameter, $L/d$, and the solvent viscosity, $\eta_0$.[48,49] In this work, we used the formula developed recently by Aragon and Flamik using the boundary element method (BE).[50] These authors evaluated the diffusion coefficients for cylinders with spherical caps, flat caps, and tubes with a thin wall. Worm-like micelles are usually represented as flexible cylinders with a spherical cap at each end. For the case of PFS based micelles, however, we have shown that micelle growth occurs from both ends.[14,40] This observation strongly suggests that the ends of PFS micelles are accessible to subsequent addition of PFS unimers, and that the micelles are best represented by cylinders with flat caps.

For cylinders with flat caps, the translational diffusion coefficients, $D_\perp$ and $D_\parallel$, are given by

$$D_\perp = \frac{kT}{4\pi\eta_0 L}(\ln(L/d) + X_\perp) \tag{10a}$$

$$D_\parallel = \frac{kT}{4\pi\eta_0 L}(2\ln(L/d) + X_\parallel) \tag{10b}$$

where

$$X_\perp(L/d) = 0.866049 - \frac{0.650602}{\sqrt{L/d}} + \frac{1.2839}{L/d} - \frac{0.397905}{(L/d)^2} - \frac{0.18332\ln(L/d)}{(L/d)^2} \tag{11a}$$

$$X_\parallel(L/d) = -0.234963 - \frac{3.14268}{\sqrt{L/d}} + \frac{4.29031}{L/d} + \frac{0.197913}{(L/d)^2} - \frac{1.96581\ln(L/d)}{(L/d)} \tag{11b}$$

while the rotational diffusion coefficient, $D_r$ (given as $Dr^\perp$ by the authors) is

$$D_r = \frac{3kT}{\eta_0 L^3}(\ln(L/d) + X_r) \tag{12}$$

with

$$X_r(L/d) = -0.480483 - \frac{1.40056}{\sqrt{L/d}} + \frac{3.91903}{L/d} - \frac{2.4528}{(L/d)^3} + \frac{0.587033}{(L/d)^4} - \frac{2.58127\ln(L/d)}{(L/d)^2} \tag{13}$$

According to Aragon and Flamik, the perpendicular and parallel diffusion coefficients and the rotational diffusion coefficient are valid when the ratio $L/d$ is larger than 1. They also showed that the precision of their numerical expression is better than 0.05%.

## RESULTS AND DISCUSSION

When cylindrical micelles of PFS block copolymers are prepared by the seeded growth procedure, the number average lengths of the micelles, $L_n$, obtained are normally proportional to the ratio $M_{uni}/M_{seeds}$, where $M_{uni}$ is the mass of block copolymer unimers added to a solution containing a mass of micelle seeds, $M_{seeds}$, and to the number average length of the seeds, $L_{n,seeds}$, as shown by the expression

$$L_n = L_{n,seeds}\left(1 + \frac{M_{uni}}{M_{seeds}}\right) \tag{14}$$

In addition, the distribution in length of the elongated micelles depends on the distribution in length of the starting seeds.[16] The experiments described here were carried out in parallel with TEM studies of micelle formation by $PFS_{50}$–$PI_{1000}$ micelles in decane and in *t*BA reported in ref 39. The solutions examined by SLS and DLS were the same solutions studied, prepared, and presented in that work.[39] In these experiments, we used seed solutions which had a narrow length distribution (in decane: $L_w$ = 57 nm, PDI = 1.12; in *t*BA: $L_w$ = 59.2, PDI = 1.17). After we present the data from SLS studies of six elongated micelle samples prepared in this way, we will compare the micelle lengths $L_w$ deduced from fitting the SLS form factor with values obtained by TEM.

**Static Light Scattering.** As mentioned above, SLS data obtained from elongated structures are well represented by HC plots of $qR_\theta/\pi M_0 Kc$ as a function of $q$.[26,27] The data reach a plateau value at high $q$, which correspond to $N_{agg/L}$. The length, $L$, of the micelles can also be evaluated when we fit the data using eq 15:

$$f(q) = \frac{P(q)\cdot q}{\pi}\cdot L\cdot N_{agg/L} \tag{15}$$

where $P(q)$ is the form factor of the structures studied. In previous publications, we have shown that HC plots of elongated micelles formed by $PFS_{48}$–$PI_{264}$ or by $PFS_{40}$–$PDMS_{480}$ in alkane solvents could be well fitted when one used the form factor of a thin rigid rod, $P(q,L)_{thin\ rod}$ defined as

$$P(q,L)_{thin\ rod} = \frac{2}{qL}\int_0^{qL}\frac{\sin(x)}{x}\,dx - \left[\frac{2}{qL}\sin\left(\frac{qL}{2}\right)\right]^2 \tag{16}$$

In the experiments described here, however, we could not obtain a satisfying fit of the HC plots obtained from solutions of $PFS_{50}$–$PI_{1000}$ micelles in decane or in *t*BA. An example of such an unsuccessful fit is given in Figure 1A, which shows the HC plot of the longest $PFS_{50}$–$PI_{1000}$ micelles in decane grown from $PFS_{50}$–$PI_{1000}$ seeds, as well as the best fit of the data using eq 15 combined with eq 16. An interesting feature of the HC representation shown in Figure 1A is that the experimental data do not increase monotonically as a function of $q$, over the full $q$ range (from 4 to 27 $\mu m^{-1}$) as we would expect from a solution of thin rigid rods. The data reach a maximum value in the mid-$q$ region (ca. 15 $\mu m^{-1}$) and then decrease slowly as $q$ increases. Interestingly, Figure 1A also shows oscillations in the data which are characteristic of a solution of rods narrow dispersed in length.

The striking difference between the HC plots obtained here from solutions of $PFS_{50}$–$PI_{1000}$ micelles and the HC plots from $PFS_{48}$–$PI_{264}$ and $PFS_{40}$–$PDMS_{480}$ micelle solutions in decane[40,37,38] mentioned in the introduction is due to the nature and the length of the corona blocks. For example, PDMS is contrast matched in decane, which means that the corona of the elongated micelle does not scatter light, while, in the case of $PFS_{48}$–$PI_{264}$ micelles, the length of the PI block is rather short and the micelle would still appear like a thin rigid


dx.doi.org/10.1021/jp210454z | J. Phys. Chem. B 2012, 116, 4328–4337

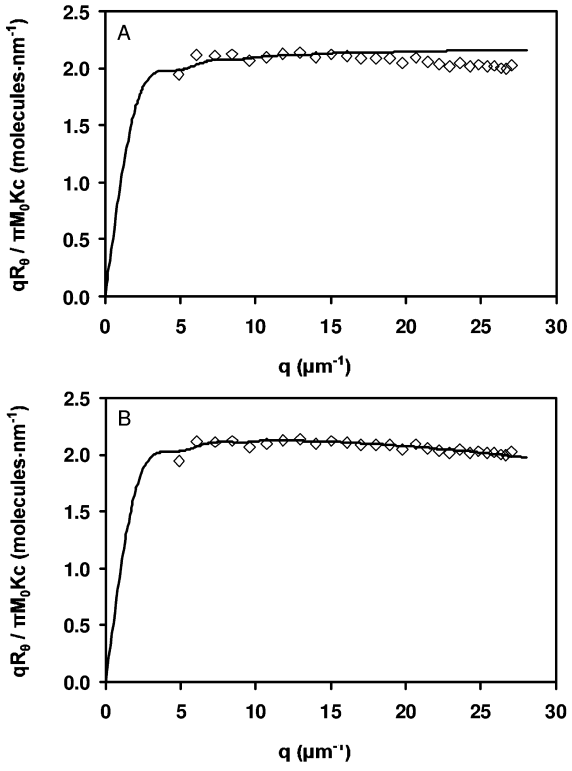


**Figure 1.** (A) Plot of $qR_\theta/\pi M_0 Kc$ as a function of $q$ for micelles grown in decane. The solid line is the best fit possible when we consider that the micelles are thin rigid rods (eq 16). (B) Fit of the same data to eq 18 for thick rigid rods with a radius cross section of $R_{SLS}$ = 24 nm. The number average length of the micelles evaluated by TEM was $L_n$ = 1400 nm and $L_w/L_n$ = 1.03, taken from ref 39.

rod. However, the PI block of $PFS_{50}$–$PI_{1000}$ is much longer, and we expect the corona to affect the scattered signal.

The scattering form factor of a cylinder of length $L$ and a circular cross section of radius, $R_{SLS}$, is given by[51]

$$P(q, L, R_{SLS})_{\text{thick rod}} = \int_0^{\pi/2} \left[ 2 \cdot \left( \frac{\sin\left(\frac{qL\cos(\alpha)}{2}\right)}{\frac{qL\cos(\alpha)}{2}} \right) \cdot J_1\left( \frac{qR_{SLS}\sin(\alpha)}{qR_{SLS}\sin(\alpha)} \right) \right]^2 \times \sin(\alpha)\, d\alpha \quad (17)$$

When the aspect ratio $(L/r)$ is large enough, eq 17 can be simplified to give

$$P(q, L, R_{SLS})_{\text{thick rod}} = P(q, L)_{\text{thin rod}} \cdot P(q, R_{SLS})_{cs} \quad (18)$$

where $P(q, L)_{\text{thin rod}}$ is given by eq 16 and $P(q, R_{SLS})_{cs}$ is given by

$$P(q, R_{SLS})_{cs} = \left( 2\frac{J_1(qR_{SLS})}{qR_{SLS}} \right)^2 \quad (19)$$

The improvement in the quality of the fit can be seen in Figure 1B, where we present the same data as in Figure 1A but fitted using eqs 15 and 18. The new fit not only reproduces the oscillations observed in the experimental data, but it also simulates the decrease of the HC plot when $q$ becomes larger than 15 $\mu m^{-1}$.

Figure 2 presents plots of $qR_\theta/\pi M_0 Kc$ versus $q$ for the six samples in decane (Figure 2A) and in *t*BA (Figure 2B). In this

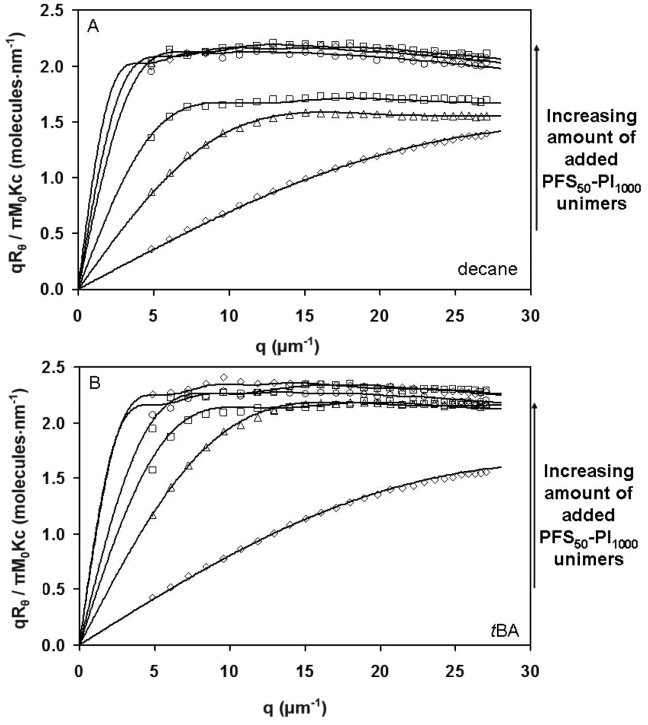


**Figure 2.** Plots of $qR_\theta/\pi M_0 Kc$ as a function of $q$ for micelles grown (A) in decane and (B) in *t*BA. The solutions were prepared by adding different amounts of $PFS_{50}$–$PI_{1000}$ unimers dissolved in THF ($c$ = 9.3 mg/mL) to solutions of $PFS_{50}$–$PI_{1000}$ seeds ($c$ = 0.02 mg/mL). The length of the starting seeds was $L_n$ = 50.9 nm in decane and $L_n$ = 50.8 nm in *t*BA. The solid lines represent the best fits of the data using the form factor of a long thick rigid rod.

figure, we also present plots of the fits to the data obtained with eqs 15 and 18. As the length of the micelles in the solutions increased, the data reached their maximum values at lower $q$. The oscillations observed in the HC plots presented in Figure 2 confirm that the micelles obtained by seeded growth from seed micelles with a narrow length distribution are themselves also narrow dispersed in length. The narrow dispersity in length of the micelles simplifies our study, since we could use eqs 15 and 18 to fit these HC plots without considering any polydispersity in the length distribution of the micelles.

The maximum observed in these HC plots requires one further comment. The form factor for semiflexible micelles also exhibits a maximum in an HC plot. Schmidt et al.[42] have shown that this maximum for semiflexible objects appears at $q^* = 1.4/R_g$. They have also shown that the ratio of the maximum over the plateau value increases with the number of Kuhn segments of the scattering structure. Long semiflexible micelles would thus lead to a more pronounced bump in the HC plots than is seen in Figures 1 and 2. Our data can be well fitted using the form factor of a thick rigid rod, and we infer that they are not semiflexible objects.

From the fits shown in Figure 2, we can calculate three important parameters describing the micelles: the weight average length of the micelle, $L_w$, the linear aggregation number, $N_{agg/L}$, and the radius of the cylinder cross section,


dx.doi.org/10.1021/jp210454z | J. Phys. Chem. B 2012, 116, 4328–4337

$R_{SLS}$. We fitted the HC plots by adjusting manually each of the three parameters, $L_w$, $R_{SLS}$, and $N_{agg/L}$. The fitting procedure is simplified by the fact that each adjustable parameter affects the HC plots in a different way. The location of the oscillations along the $q$ axis allows one to determine the micelle length $L_w$, the downward slope at high $q$ is affected by the value of $R_{SLS}$, and the height of the plot leads to the value of $N_{agg/L}$.

The evolution of these three parameters as a function of $M_{uni}/M_{seeds}$ is shown in Figure 3. In Figure 3A, we present the evolution of the weight average length evaluated by SLS as a function of $M_{uni}/M_{seeds}$ for the micelles grown in decane and in *t*BA. In this figure, we also plotted the weight average length deduced from TEM measurements, $L_w^{TEM}$, for the same micelle solutions (data taken from ref 39), as well as the expected length deduced from eq 14, which considers that all the unimers grew on the existing seeds. The length values obtained from TEM image analysis are in excellent agreement with the values deduced from SLS measurements, but SLS provides supplementary information about the micelles grown in decane and in *t*BA. From the fit of HC plots, we can monitor the evolution of $N_{agg/L}$ as a function of $M_{uni}/M_{seeds}$, as presented in Figure 3B. One can see that the linear aggregation numbers of the micelles grown in *t*BA and decane are similar. Moreover, in both cases, $N_{agg/L}$ increased slightly from 2 to 2.5 unimers/nm when the ratio $M_{uni}/M_{seeds}$ was increased. Figure 3C shows the evolution of the radius of the micelle cross section as a function of $M_{uni}/M_{seeds}$. Here again, the similarities between the values obtained from the micelles grown in decane and those grown in *t*BA are striking. In both solvents, the radii of the micelle cross sections were close to 22 nm and did not seem to be influenced by the amount of unimer added or the length of the micelles formed.

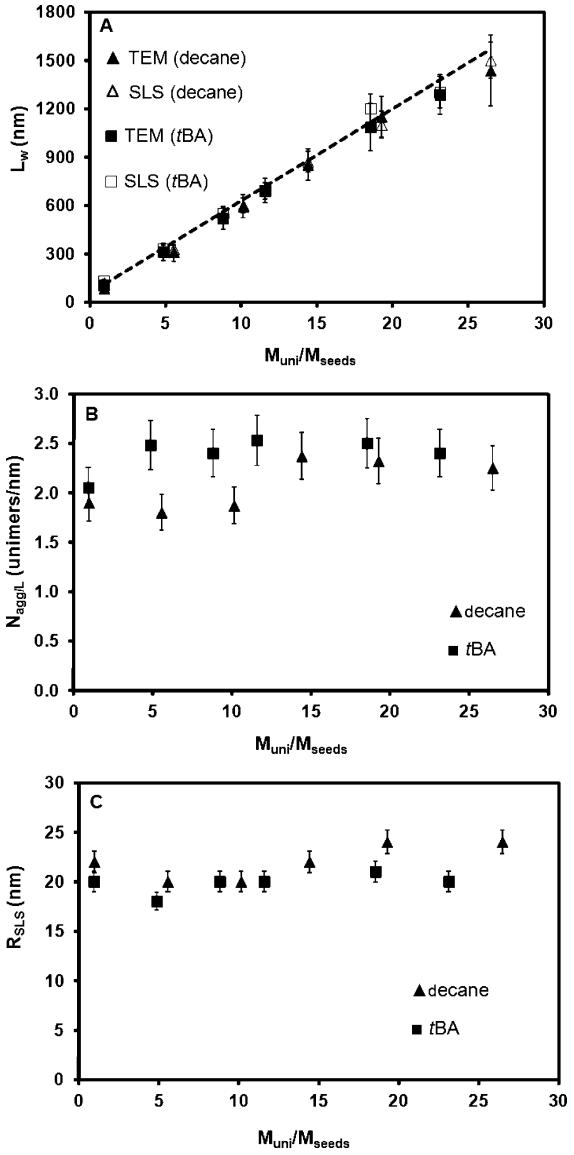


**Figure 3.** (A) Plot of the weight average length of $PFS_{50}$−$PI_{1000}$ micelles grown in decane (triangles) and in *t*BA (squares) as a function of $M_{uni}/M_{seeds}$ evaluated by SLS (open symbols) and by TEM (filled symbols) (TEM data from ref 39). The dashed line represents the expected weight average length if 100% of the added unimers grow on the seeds. (B) Plot of the linear aggregation number, $N_{agg/L}$, as a function of $M_{uni}/M_{seeds}$ obtained by SLS for micelles grown in decane (triangles) and in *t*BA (squares). (C) Plot of the radius of the micelle cross section, $R_{SLS}$, as a function of $M_{uni}/M_{seeds}$ deduced from the fits of the SLS data from micelles grown in decane (triangle symbols) and *t*BA (square symbols).

The results obtained from static light scattering experiments suggest that the solvent has little influence on the micelle structure and the conformation of the corona chains, since $N_{agg/L}$ and $R_{SLS}$ are almost identical in decane and in *t*BA. The fact that $R_{SLS}$ is the same for micelles dispersed in decane and in *t*BA is surprising because the total solubility parameter of *t*BA ($\delta_{tBA}$ = 16.6 $MPa^{1/2}$) is closer to the solubility parameter of polyisoprene ($\delta_{PI}$ = 17 $MPa^{1/2}$) than decane is ($\delta_{decane}$ = 15.8 $MPa^{1/2}$), and one would expect the PI corona to be more swollen when the micelles are dispersed in the better solvent.

**Dynamic Light Scattering.** An important advantage of modern multiangle light scattering instrumentation is that one can perform SLS and DLS experiments simultaneously.[52] In SLS, one evaluates the average intensity of the scattered signal, whereas, in DLS, one analyzes the fluctuations in the scattered intensity of the same signal, due to the motion of the scatterers in solution. As we have shown earlier, the autocorrelation function of the scattered intensity decays exponentially with time (eq 5), and the evolution of the average decay rate as a function of the scattering angle provides information about the diffusion of the scatterers in solution (eq 9). Since the diffusion of a scattering particle is strongly related to its shape and its dimensions (eqs 10 and 12), DLS provides an alternative way to evaluate the radius of the micelle cross section.

Figure 4 shows the evolution of $\Gamma_1/q^2$ as a function of $qL$ for all the micelles in decane (Figure 4A) and in *t*BA (Figure 4B), with the solid lines representing the best fits obtained using Maeda's equation (eq 9). One can see in this plot that the Maeda equation approximates very well the variation of the reduced cumulant, $\Gamma_1/q^2$, versus $qL$ for all the micelle solutions studied. This agreement is even more impressive when we consider the fact that the length of the micelles we were studying varied from 120 to 1500 nm.

At low values of $qL$, the reduced cumulant should be constant and equal to the translational diffusion coefficient, as expected for spherical objects. As $qL$ increases, the reduced cumulant reaches another plateau value equal to $\Gamma_1/q^2 = D_\perp + L^2/12D_r$. The Maeda equation depends on the values of the translational and rotational diffusion coefficients, which can be adjusted using hydrodynamic considerations.[48,50] In the case of rigid cylinders, the diffusion coefficients depend only on the ratio $L/d$, where $L$ is the length of the cylinder and $d$, the


dx.doi.org/10.1021/jp210454z | J. Phys. Chem. B 2012, 116, 4328−4337

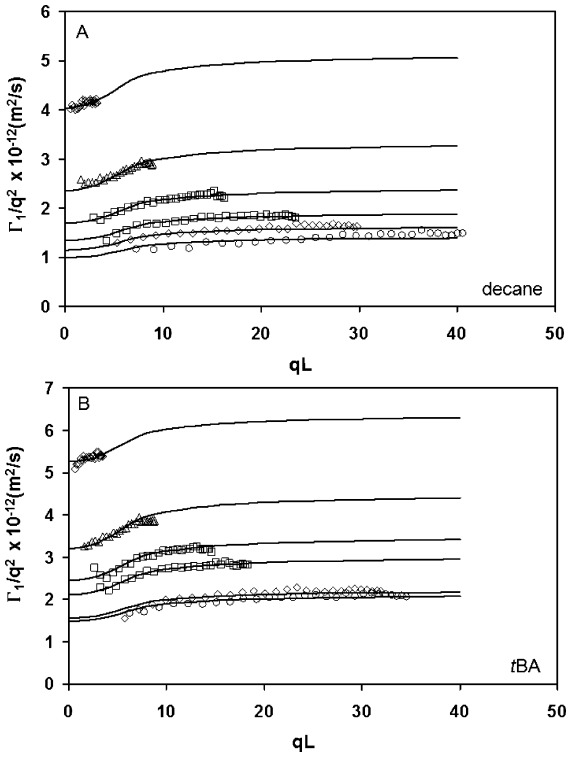


**Figure 4.** Plots of $\Gamma_1/q^2$ as a function of $qL$ for micelles grown in (A) decane and (B) *t*BA. The value of $L$ corresponds to the weight average length, $L_w$, evaluated from the fits of SLS data. The solid lines correspond to the best fits obtained from Maeda (eq 9).

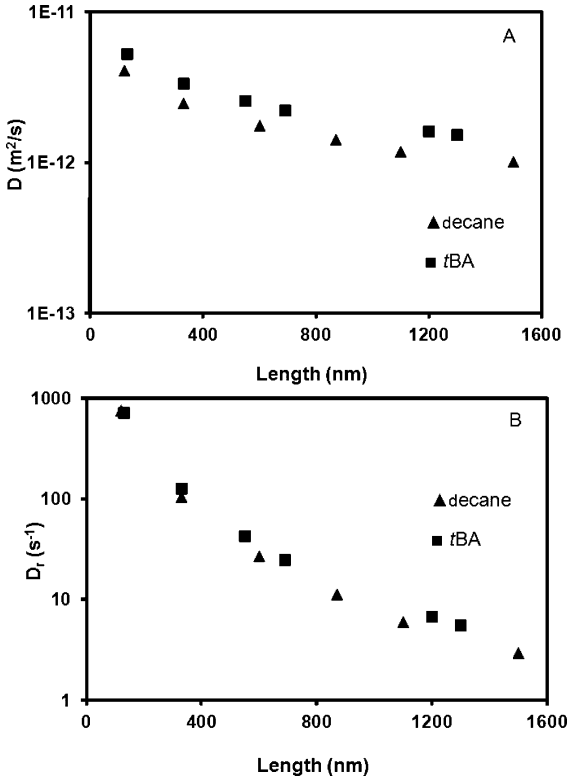


**Figure 5.** Semilogarithmic plots of (A) the translational diffusion coefficient, $D$, as a function of micelle length, $L$, in *t*BA (square symbols) and in decane (triangles); (B) the rotational diffusion coefficient, $D_r$, as a function of micelle length, $L$, in *t*BA (square symbols) and in decane (triangles).

diameter of its cross section (eqs 10−13). We used the length determined by SLS as a fixed parameter. Since the length values obtained independently by SLS and TEM were in excellent agreement, we are confident that these data are meaningful (in Table S1 in the Supporting Information, we compare the values of $L_n$, $L_w$, and the $z$-average length of the micelles, $L_z$). We, then, varied the value of the diameter of the cross section using the Aragon and Flamik relationships (eqs 11 and 13), to fit the data shown in Figure 4.

Figure 5 shows the logarithmic evolution of the translational (Figure 5A) and rotational (Figure 5B) diffusion coefficient as a function of micelle length from micelles grown in *t*BA and in decane (the data are summarized in Table S2 in the Supporting Information). Both diffusion coefficients decrease monotonically with the length of the micelles. These values are in good agreement with those we found in a previous study of 1 $\mu$m long $PFS_{40}$−$PDMS_{480}$ micelles in decane, where $D = 2.01 \times 10^{-12}$ m$^2$ s$^{-1}$ and $D_r = 13$ s$^{-1}$, deduced using Broersma expressions.[37] For comparison, in decane, $PFS_{50}$−$PI_{1000}$ micelles with a length of 1.1 $\mu$m have a translational diffusion coefficient of $D = 1.18 \times 10^{-12}$ m$^2$ s$^{-1}$ and a rotational diffusion coefficient of $D_r = 6$ s$^{-1}$.

The values of diffusion coefficients we deduced from the fits of the reduced cumulant versus $qL$ are also on the same order of magnitude as the diffusion coefficients of other elongated molecules. The value reported for the translational diffusion of collagen molecules, which are 240 nm long and have a very small cross section diameter (1.36 nm), is ca. $9 \times 10^{-12}$ m$^2$ s$^{-1}$, while the rotational diffusion coefficient is close to 1100 s$^{-1}$.[32] Tobacco mosaic virus (TMV) is even more interesting for us to compare with because the length (300 nm) and the cross section diameter (18 nm) of this virus of cylindrical shape are in the range of the PFS−PI micelles we are studying.[53] By dynamic light scattering, Lehner et al.[54] evaluated the TMV translational diffusion coefficient to be $4 \times 10^{-12}$ m$^2$ s$^{-1}$, while the rotational diffusion coefficient was equal to 300 s$^{-1}$. In comparison, we observed that $PFS_{50}$−$PI_{1000}$ micelles which are 330 nm long have a translational diffusion coefficient of $2.3 \times 10^{-12}$ m$^2$ s$^{-1}$ and a rotational diffusion coefficient of 105 s$^{-1}$.

For a solution of cylindrical scattering objects, in unpolarized (VU) and vertically (VV) polarized configurations, one would expect to observe two distinguishable decay rates. The main decay rate, $\Gamma_{main}$, is related to the translational diffusion coefficient of the rod, $\Gamma_{main} = q^2D$, while the faster decay rate is due to the contribution of both the rotational and translational diffusion coefficients, and $\Gamma_{fast} = q^2D + 6D_r$. The relative contribution of the fast decay rate should increase as the scattering angle increases.[32] In depolarized light scattering (VH), the purely translational mode is cut off and only one decay rate is observed, $\Gamma_{dep} = q^2D + 6D_r$. A convenient way to observe the presence of one or two decay rates is to perform an inverse-Laplace transform of the autocorrelation function, using a procedure such as CONTIN. This type of analysis should produce a peak corresponding to each decay rate.[55] However, for elongated micelles obtained from the self-assembly of PFS based block copolymers in dilute solution, the depolarized scattered signal is very weak. The depolarized ratio is lower than 0.5%, and one observes only a single decay rate at all scattering angles. For example, in previous work, we studied a solution of $PFS_{40}$−$PDMS_{480}$ micelles in decane by polarized dynamic light scattering, but we could not observe the fast decay rate. Using the Maeda equation, however, we found that


dx.doi.org/10.1021/jp210454z | J. Phys. Chem. B 2012, 116, 4328−4337

the value of the rotational diffusion coefficient was low ($D_r$ = 13 $s^{-1}$), and we argued that the rotational diffusion coefficient might be too low to be observable. Later, Korczagin et al.[56] studied the evolution of the autocorrelation function of the depolarized intensity signal of a solution of elongated PFS–PMMA micelles in acetone. These authors also mentioned that the decay rate obtained by polarized and depolarized light scattering were similar, and they also explained their results by considering that the rotational diffusion coefficient was too low to influence the decay rate.

In the present work, we studied solutions of micelles with different lengths, and the rotational diffusion coefficient values we deduced from the Maeda equation ranged from ca. 5 $s^{-1}$ for the longest micelles to ca. 800 $s^{-1}$ for the shortest. However, by CONTIN analysis, we could not distinguish the contribution from the rotational diffusion coefficient for any of the samples at any angles. This result is rather surprising because, for micelles less than 600 nm long, the rotational diffusion coefficient was larger than 40 $s^{-1}$, which should be large enough to be distinguishable.

Figure 6 shows the evolution of the radius of the micelle cross section, $R_{DLS}$, deduced from the fits of the reduced

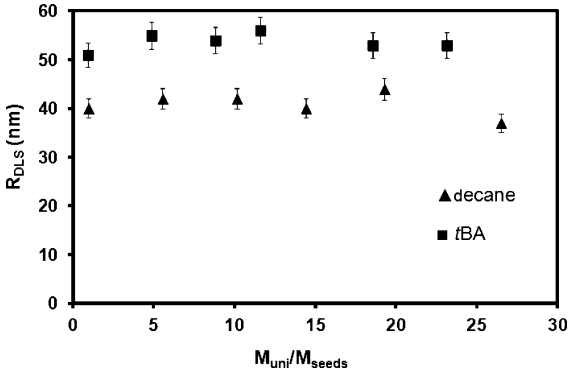


**Figure 6.** Plot of the radius of the micelle cross section, $R_{DLS}$, as a function of $M_{uni}/M_{seeds}$ deduced from the fits of the reduced cumulant from micelles grown in decane (triangle symbols) and *t*BA (square symbols).

cumulant shown in Figure 4. One can observe in Figure 6 that the radius of the cross section of the micelles in decane and in *t*BA does not depend on the ratio $M_{uni}/M_{seeds}$, or, in other words, on the micelle length, and fluctuates around an average value of 40 nm in decane and 50 nm in *t*BA. There are two important facts that one learns from this plot. First, the radius obtained by DLS of the cross section of the micelles in decane is significantly smaller than in *t*BA. Second, this radius is more than 2 times larger than the radius deduced from the SLS fitting.

The difference between $R_{DLS}$ and $R_{SLS}$ is most likely a consequence of the density distribution of the corona in the radial direction. As the corona chains protrude from the core surface in the radial direction, they become more diffuse, more swollen by the solvent. Thus, the corona is expected to be denser close to the center of the micelle than at its fringe. There are several equations available to model the change in density in microgels,[57] along the radial axis of bottle-brush polymers,[58] or of the corona of micelles.[59] For example, Gohr et al.[59] proposed to fit the density profile of poly(styrene-*b*-butadiene) (PS–PB) spherical micelles using the density profile, $n(r)$, defined by $n(r) = r - x/(\exp((r - ra)/s) + 1)$; when $x$ = 4/3, the equation is close to the model developed by Daoud and Cotton, and when $x$ = 0, the equation is equal to the Fermi–Dirac (FD) distribution function used by Won et al.[60]

The fact that $R_{DLS}$ is larger for micelles grown in *t*BA than in decane while $R_{SLS}$ values are similar in both solvents might seem counterintuitive. However, we want to remind the reader that the value of d$n$/d$c$ for PI is larger in *t*BA (0.146 mL/g) than in decane (0.120 mL/g), and for this reason, at the same amount of swelling, the corona would have less contrast in decane than in *t*BA. To represent this effect, we plot in Figure 7

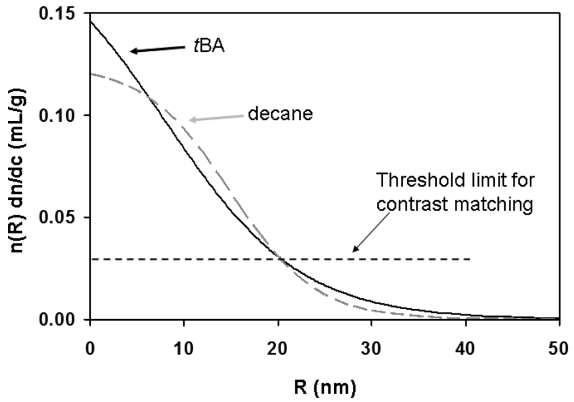


**Figure 7.** Plot of $n(R)$ d$n$/d$c$ as a function of radial distance, $R$, of the rod main axis for $PFS_{50}$–$PI_{1000}$ micelles in decane (black line) and in *t*BA (dashed gray line). The dashed line represents the limit below which the corona is considered as contrast matched.

the product $\rho(r) = n(r)$ d$n$/d$c$, of the density profile multiplied by the value of d$n$/d$c$ of the PI corona in each solvent, *t*BA and decane. The density profile is represented by the Fermi–Dirac distribution function, and the values of the parameters we used to plot both curves were purely arbitrary. Figure 7, however, gives an interesting estimation of the difference in the density of the corona in decane and in *t*BA along the radial direction.

Won et al.[60] studied elongated wormlike micelles of PEO–PB (PEO = poly(ethylene oxide)) in water, a selective solvent for the PEO block, using small angle neutron scattering (SANS). With SANS, these authors could distinguish the PB core of the worm-like micelle from the PEO corona, and they modified the form factor of a worm-like micelle by introducing a term accounting for the density profile of the corona. Unfortunately, with light scattering, we cannot distinguish the core from the corona in the radial direction and we cannot further quantify the degree of swelling of the corona in *t*BA and in decane.

As a final note, we would like to raise an interesting observation concerning the difference in the density profiles of the corona in *t*BA and decane. One might think that the density profile would not only be related to the interaction between the solvent and the PI chains but also to a difference in the chain packing inside the crystalline core of the micelles.[61,62] For example, Cambridge et al.[23] showed that, for a series of samples, the linear aggregation number of PFS-based elongated micelles decreased as the length of the corona block increased, presumably to comply with the increase in steric hindrance in the corona. We also observed that the linear aggregation number we obtained by SLS for $PFS_{50}$–$PI_{1000}$ micelles in decane, 2.5 chains $nm^{-1}$, is lower than the value previously obtained for $PFS_{48}$–$PI_{264}$ in decane, 3.5 chains $nm^{-1}$. However, we did not observe any obvious difference in $N_{agg/L}$ in decane


dx.doi.org/10.1021/jp210454z | J. Phys. Chem. B 2012, 116, 4328–4337

and in *t*BA despite the fact the PI corona chains are more stretched in *t*BA than in decane. Using a simple blob argument, one might think that the stretching of the PI chains would decrease the repulsion inside the corona (by decreasing the blob size), allowing for a better packing of the PFS chains and increasing $N_{agg/L}$. The fact that we do not observe such a behavior suggests that there are subtle differences between the cores of the micelles grown in *t*BA and those grown in decane, which would compensate for the stretching of the corona chains. To have a better understanding of the solvent effect on PFS based block copolymer, we have investigated the formation of PFS based micelles in a mixture of decane and *t*BA solvents. The results are however beyond the scope of the present work and will be published in the future.

## SUMMARY

In previous experiments reported in the literature, when elongated structures were studied by static light scattering, the diameters of their cross sections were too thin to be observed. In other examples involving worm-like micelles, their flexibility played an important role in determining the shape of the angular-dependent static light scattering signal. In this work, we studied a series of $PFS_{50}$–$PI_{1000}$ micelles in *t*BA and in decane. This block copolymer formed rigid one-dimensional micelles with a cross section sufficiently thick to affect the static light scattering signal. These data could be fitted to yield values of the cross section of the micelles. From SLS experiments on a series of micelles of different length, we found that both the linear aggregation number, $N_{agg/L}$, and the magnitude of the cross section of the micelles, $R_{SLS}$, were almost independent of the length of the micelles. In addition, both values were similar for micelles formed in decane and in *t*BA. DLS experiments, however, showed that the hydrodynamic radius of the cross section was larger for micelles grown in *t*BA than for those grown in decane. We infer that the difference between the cross sections obtained from SLS and DLS data fitting is due to a difference in the density profile of the PI block forming the micelle corona in the two solvents.

## ASSOCIATED CONTENT

### Supporting Information

A plot of the overlap concentration of the micelles as a function of the micelle length (Figure S1), the values of $D_{\parallel}$, $D_{\perp}$, and $D_r$ obtained by fitting $\Gamma_1/q^2$ as a function of $q^2$ (Table S1), and the values of $L_n$, $L_w$, and $L_z$ evaluated by TEM image analysis (Table S2). This material is available free of charge via the Internet at http://pubs.acs.org.

## AUTHOR INFORMATION

### Corresponding Author

*E-mail: mwinnik@chem.utoronto.ca (M.A.W.); ian.manners@bristol.ac.uk (I.M.).

### Notes

The authors declare no competing financial interest.

## ACKNOWLEDGMENTS

The authors thank NSERC Canada for their support of this research. I.M. thanks the European Union for a Marie Curie Chair and an Advanced Investigator Grant and the Royal Society for a Wolfson Research Merit Award. G.G. would also like to thank Professor S. Aragon (UC San Francisco) for fruitful discussions.

## REFERENCES

(1) Riess, G. *Prog. Polym. Sci.* **2003**, *28*, 1107–1170.
(2) Bang, J.; Jain, S.; Li, Z.; Lodge, T. P.; Pedersen, J. S.; Kesselman, E.; Talmon, Y. *Macromolecules* **2006**, *39*, 1199–1208.
(3) Alexandridis, P.; Lindman, B. *Amphiphilic Block Copolymers*; Elsevier Science B. V.: Amsterdam, The Netherlands, 2000.
(4) Hamley, I. *Copolymers in Solution*; John Wiley and Sons Ltd.: Chichester, West Sussex, England, 2005.
(5) O'Reilly, R. *Philos. Trans. R. Soc., A* **2007**, *365*, 2863–2878.
(6) Won, Y.-Y.; Davis, H. T.; Bates, F. S. *Science* **1999**, *283*, 960–963.
(7) Discher, B. M.; Won, Y.-Y.; Ege, D. S.; Lee, J. C.-M.; Bates, F. S.; Discher, D. E.; Hammer, D. A. *Science* **1999**, *284*, 1143–1146.
(8) Lin, E. K.; Gast, A. P. *Macromolecules* **1996**, *29*, 4432–4441.
(9) Vilgis, T.; Halperin, A. *Macromolecules* **1991**, *24*, 2090–2095.
(10) Geng, Y.; Dalhaimer, P.; Cai, S.; Tsai, R.; Tewari, M.; Minko, T.; Discher, D. E. *Nat. Nanotechnol.* **2007**, *2*, 249–255.
(11) Thio, Y. S.; Wu, J.; Bates, F. S. *Macromolecules* **2006**, *39*, 7187–7189.
(12) Wang, H.; Patil, A. J.; Liu, K.; Petrov, S.; Mann, S.; Winnik, M. A.; Manners, I. *Adv. Mater.* **2009**, *21*, 1805–1808.
(13) Massey, J.; Power, K. N.; Manners, I.; Winnik, M. A. *J. Am. Chem. Soc.* **1998**, *120*, 9533–9540.
(14) Gadt, T.; Ieong, N.; Cambridge, G.; Winnik, M.; Manners, I. *Nat. Mater.* **2009**, *8*, 144–150.
(15) Cao, L.; Manners, I.; Winnik, M. A. *Macromolecules* **2002**, *35*, 8258–8260.
(16) (a) Gilroy, J. B.; Gädt, T.; Whittell, G. R.; Chabanne, L.; Mitchels, J. M.; Richardson, R. M.; Winnik, M. A.; Manners, I. *Nat. Chem.* **2010**, *2*, 566–570. (b) Gilroy, J. B.; Rupar, P. A.; Whittell, G. R.; Chabanne, L.; Terrill, N. J.; Winnik, M. A.; Manners, I.; Richardson, R. M. *J. Am. Chem. Soc.* **2011**, *133*, 17056–17062.
(17) He, F.; Gadt, T.; Jones, M.; Scholes, G.; Manners, I.; Winnik, M. *Macromolecules* **2009**, *42*, 7953–7960.
(18) Lazzari, M.; Scalarone, D.; Vazquez-Vazquez, C.; López-Quintela, M. A. *Macromol. Rapid Commun.* **2008**, *29*, 352–357.
(19) Mihut, A. M.; Drechsler, M.; Möller, M.; Ballauff, M. *Macromol. Rapid Commun.* **2010**, *31*, 449–453.
(20) Petzetakis, N.; Dove, A. P.; O'Reilly, R. K. *Chem. Sci.* **2011**, *2*, 955–960.
(21) Patra, S. K.; Ahmed, R.; Whittell, G. R.; Lunn, D. J.; Dunphy, E. L.; Winnik, M. A.; Manners, I. *J. Am. Chem. Soc.* **2011**, *133*, 8842–8845.
(22) Wilhelm, J.; Frey, E. *Phys. Rev. Lett.* **1996**, *77*, 2581–2584.
(23) Cambridge, G.; Guerin, G.; Manners, I.; Winnik, M. A. *Macromol. Rapid Commun.* **2010**, *31*, 934–938.
(24) Dalhaimer, P.; Bates, F. S.; Discher, D. E. *Macromolecules* **2003**, *36*, 6873–6877.
(25) LaRue, I.; Adam, M.; da Silva, M.; Sheiko, S. S.; Rubinstein, M. *Macromolecules* **2004**, *37*, 5002–5005.
(26) Holtzer, A. *J. Polym. Sci.* **1955**, *17*, 432–434.
(27) Casassa, E. *J. Chem. Phys.* **1955**, *23*, 596–597.
(28) Merkle, G.; Auerbach, S.; Burchard, W.; Lindner, A.; Wegener, G. *J. Appl. Polym. Sci.* **1992**, *45*, 407–415.
(29) Yan, Y.; de Keizer, A.; Martens, A. A.; Oliveira, C. L. P.; Pedersen, J. S.; de Wolf, F. A.; Drechsler, M.; Cohen Stuart, M. A.; Besseling, N. A. M. *Langmuir* **2009**, *25*, 12899–12908.
(30) Glatter, O. *J. Appl. Crystallogr.* **1980**, *13*, 577–584.
(31) Terech, P.; Dourdain, S.; Bhat, S.; Maitra, U. *J. Phys. Chem. B* **2009**, *113*, 8252–8267.
(32) Aragon, S. R.; Pecora, R. *J. Chem. Phys.* **1985**, *82*, 5346–5353.
(33) Claire, K.; Pecora, R. *J. Phys. Chem. B* **1997**, *101*, 746–753.
(34) Castelletto, V.; Hamley, I. W.; Harris, P. J. F.; Olsson, U.; Spencer, N. *J. Phys. Chem. B* **2009**, *113*, 9978–9987.
(35) Shen, C. L.; Scott, G. L.; Merchant, F.; Murphy, R. M. *Biophys. J.* **1993**, *65*, 2383–2395.
(36) Phalakornkul, J. K.; Gast, A. P.; Pecora, R. *Macromolecules* **1999**, *32*, 3122–3135.
(37) Guérin, G.; Raez, J.; Manners, I.; Winnik, M. A. *Macromolecules* **2005**, *38*, 7819–7827.

(38) Guérin, G.; Wang, H.; Manners, I.; Winnik, M. A. *J. Am. Chem. Soc.* **2008**, *130*, 14763−14771.
(39) Qi, F.; Guerin, G.; Cambridge, G.; Xu, W.; Manners, I.; Winnik, M. A. *Macromolecules* **2011**, *44*, 6136−6144.
(40) Wang, X.; Guerin, G.; Wang, H.; Wang, Y.; Manners, I.; Winnik, M. A. *Science* **2007**, *317*, 644−647.
(41) Kratochvil, P. *Classical Light Scattering from Polymer Solutions*; Polymer Science Library 5; Elsevier: Amsterdam, New York, 1987.
(42) Schmidt, M.; Paradossi, G.; Burchard, W. *Makromol. Chem. Rapid Commun.* **1985**, *6*, 767−772.
(43) Jakeman, E. In *Photon Correlation and Light Beating Spectroscopy*; Cummins, H. Z., Pike, E. R., Eds; Plenum Press: New York, 1974.
(44) Frisken, B. J. *Appl. Opt.* **2001**, *40*, 4087−4091.
(45) Hassan, P. A.; Kulshreshtha, S. K. *J. Colloid Interface Sci.* **2006**, *300*, 744−748.
(46) Koppel, D. E. *J. Chem. Phys.* **1972**, *57*, 4814−4820.
(47) Maeda, T.; Fujime, S. *Macromolecules* **1984**, *17*, 1157−1167.
(48) (a) Broersma, S. *J. Chem. Phys.* **1960**, *32*, 1626−1631. (b) Broersma, S. *J. Chem. Phys.* **1960**, *32*, 1632−1635. (c) Broersma, S. *J. Chem. Phys.* **1981**, *74*, 6989−6990.
(49) (a) Tirado, M. M.; de la Torre, J. G. *J. Chem. Phys.* **1979**, *71*, 2581−2587. (b) Tirado, M. M.; de la Torre, J. G. *J. Chem. Phys.* **1980**, *73*, 1986−1993.
(50) Aragon, S. R.; Flamik, D. *Macromolecules* **2009**, *42*, 6290−6299.
(51) Glatter, O. In *Small Angle X-Ray Scattering*; Glatter, O., Kratky, O., Eds.; Academic Press: London, 1982.
(52) Bantle, S.; Schmidt, M.; Burchard, W. *Macromolecules* **1982**, *15*, 1604−1609.
(53) Cush, R.; Dorman, D.; Russo, P. S. *Macromolecules* **2004**, *37*, 9577−9584.
(54) Lehner, D.; Lindner, H.; Glatter, O. *Langmuir* **2000**, *16*, 1689−1695.
(55) (a) Provencher, S. W. *J. Chem. Phys.* **1976**, *64*, 2772−2777. (b) Provencher, S. W. *Comput. Phys. Commun.* **1982**, *27*, 213−227. (c) Provencher, S. W. *Comput. Phys. Commun.* **1982**, *27*, 229−242.
(56) Korczagin, I.; Hempenius, M. A.; Fokkink, R. G.; Cohen Stuart, M. A.; Al-Hussein, M.; Bomans, P. H. H.; Frederik, P. M.; Vancso, G. J. *Macromolecules* **2006**, *39*, 2306−2315.
(57) Antonietti, M.; Bremser, W.; Schmidt, M. *Macromolecules* **1990**, *23*, 3796−3805.
(58) Rathgeber, S.; Pakula, T.; Wilk, A.; Matyjaszewski, K.; Beers, K. L. *J. Chem. Phys.* **2005**, *122*, 124904.
(59) Gohr, K.; Schärtl, W.; Willner, L.; Pyckhout-Hintzen, W. *Macromolecules* **2002**, *35*, 9110−9116.
(60) Won, Y.-Y.; Davis, H. T.; Bates, F. S.; Agamalian, M.; Wignall, G. D. *J. Phys. Chem. B* **2000**, *104*, 7134−7143.
(61) Herman, J.; Jérome, R.; Teyssié, P.; Gervais, M.; Gallot, B. *Makromol. Chem.* **1981**, *182*, 997−1008.
(62) Birshtein, T. M.; Zhulina, E. B. *Polymer* **1990**, *31*, 1312−1320.